Thermally driven smoothening of molecular thin films: Structural transitions in n-alkane layers studied in real-time

Linus Pithan, Eduard Meister, Chenyu Jin, Christopher Weber, Anton Zykov, Katrein Sauer, Wolfgang Brütting, Hans Riegler, Andreas Opitz, and Stefan Kowarik

Articles you may be interested in

Chain-length dependent growth dynamics of n-alkanes on silica investigated by energy-dispersive x-ray reflectivity in situ and in real-time
J. Chem. Phys. **136**, 204709 (2012); 10.1063/1.4719530

The impact of the density and type of reactive sites on the characteristics of the atomic layer deposited W N x C y films
J. Appl. Phys. **99**, 063515 (2006); 10.1063/1.2182074

Growth kinetics, structure, and morphology of para-quaterphenyl thin films on gold(111)
J. Chem. Phys. **121**, 2272 (2004); 10.1063/1.1767154

Optical and structural studies of films grown thermally on zirconium surfaces
J. Appl. Phys. **91**, 9375 (2002); 10.1063/1.1476079

Model for the $\alpha \rightarrow \beta_1$ phase transition in phthalocyanine thin films
J. Appl. Phys. **91**, 3632 (2002); 10.1063/1.1446218

Thermally driven smoothening of molecular thin films: Structural transitions in n-alkane layers studied in real-time

Linus Pithan,[1] Eduard Meister,[2] Chenyu Jin,[3] Christopher Weber,[1] Anton Zykov,[1] Katrein Sauer,[1] Wolfgang Brütting,[2] Hans Riegler,[3] Andreas Opitz,[1] and Stefan Kowarik[1,a)]

[1]*Institut für Physik, Humboldt-Universität zu Berlin, 12489 Berlin, Germany*
[2]*Institut für Physik, Universität Augsburg, 86135 Augsburg, Germany*
[3]*Max-Planck-Institut für Kolloid- und Grenzflächenforschung, 14476 Potsdam-Golm, Germany*

We use thermal annealing to improve smoothness and to increase the lateral size of crystalline islands of n-tetratetracontane (TTC, $C_{44}H_{90}$) films. With *in situ* x-ray diffraction, we find an optimum temperature range leading to improved texture and crystallinity while avoiding an irreversible phase transition that reduces crystallinity again. We employ real-time optical phase contrast microscopy with sub-nm height resolution to track the diffusion of TTC across monomolecular step edges which causes the unusual smoothing of a molecular thin film during annealing. We show that the lateral island sizes increase by more than one order of magnitude from 0.5 μm to 10 μm. This desirable behavior of 2d-Ostwald ripening and smoothing is in contrast to many other organic molecular films where annealing leads to dewetting, roughening, and a pronounced 3d morphology. We rationalize the smoothing behavior with the highly anisotropic attachment energies and low surface energies for TTC. The results are technically relevant for the use of TTC as passivation layer and as gate dielectric in organic field effect transistors. © *2015 AIP Publishing LLC.* [http://dx.doi.org/10.1063/1.4934501]

INTRODUCTION

Thermal annealing is an important process to improve structural and functional properties of molecular thin films. The increased temperature during the annealing process often helps to heal crystal defects and to increase crystallite sizes.[1] However, the structural definition at interfaces and surfaces may also decrease due to molecular diffusion, dewetting, and roughening.[2,3] Organic molecular beam deposition (OMBD), in particular, often leads to kinetically limited, non-equilibrium structures and postgrowth annealing, therefore, can significantly influence morphology and crystal structure.[4] Here, we study in detail the annealing of alkane thin films using real-time techniques. Alkane molecules with their simple, rod-like molecular shape are a model system for more complex chain-like organic molecules[5–7] and are also important building blocks, e.g., as side chains of polymers and can dominate their crystallisation behavior.[8,9]

Beyond its importance as a generic model system for fundamental molecular processes, tetratetracontane (TTC), in particular, is also of technological importance in organic electronics as an encapsulation material for transistors and biosensors in an aqueous environment,[10,11] where the active layer is completely wetted by TTC and therefore fully encapsulated.

In a different application, TTC has been incorporated in field-effect transistors as a smooth gate dielectric on top of a silicon gate.[12–14] In such devices, a TTC layer beneath the active molecular layer is used to passivate traps at the substrate oxide surface and further leads to improved growth and larger grain sizes of the on-top deposited semiconducting film. In this application, it has been found that the performance of ambipolar field-effect transistors can be improved by using smoothed TTC layers.[15–17] The grain size of the on-top deposited semiconducting film depends on the grain size of the underlying TTC layer. Therefore, in addition to the goal of achieving a fundamental understanding of organic thin film annealing, there is also a technological demand to maximize the TTC grain size.

TTC films[18] and single crystals[19–22] prepared from melts have been analysed before and several crystal structures have been reported in the literature. X-ray studies on $C_{44}H_{90}$ and structural changes of alkanes near their melting point range back as far as 1930 by Müller and are still subject of recent studies.[18,19] Single crystals grown from solution show a monoclinic crystal structure with a *d*-spacing of roughly 52 Å.[21,23–25] When exposed to temperatures near the alkane melting temperature, a transformation into an orthorhombic structure[7,18,23–27] with an increased *d*-spacing of roughly 58 Å can be achieved. In addition, a triclinic phase[21] and also a rotator phase[28] have been reported. Unlike most materials, alkanes feature a surface freezing behavior resulting in a higher temperature of the ordering transition in two-dimensional than in three dimensional systems.[29,30] Due to the surface freezing effect, the melting point of the surface layer of an alkane melt is increased compared to the bulk material.[31] This behaviour has been studied in detail by Ocko *et al.* who also found a remarkably wide range lateral crystalline order in surface-frozen alkane monolayers (MLs) of ~1 μm.[32,33]

In this paper, we show that through annealing we can achieve molecular thin films that have both large crystalline

---

a)Author to whom correspondence should be addressed. Electronic mail: stefan.kowarik@physik.hu-berlin.de

143, 164707-1

domains, and, importantly, also feature a smooth surface morphology at the same time. However, heating beyond a phase transition reduces the crystallinity again, so that a trade-off between crystallinity and molecularly flat island size has to be found. We relate the strongly anisotropic attachment energies of TTC to its annealing behaviour and show that anisotropic attachment energies can be used for interface engineering with optimisation of both morphology and crystallinity within the correct temperature range.

EXPERIMENTAL DETAILS

TTC (purity > 99%) was purchased from Sigma-Aldrich and used without further purification. TTC molecules have been evaporated and deposited in an organic molecular beam deposition setup with a base pressure of $1.7 \cdot 10^{-7}$ mbar onto silicon wafers with either a native oxide or a 300 nm thermal oxide layer. After deposition, the TTC coated wafers were transported to a glove-box via a transfer system and stored under nitrogen atmosphere. In order to improve the contrast in reflection optical microscopy, Si wafers with dry, thermally grown 300 nm SiO_x layer (Siegert) were used for additional samples.

For time-resolved annealing studies, we applied reflection optical microscopy to the TTC thin films and achieved contrast between molecular MLs with heights below 1 nm. In the setup, an Olympus AX70 microscope with 100× magnification illuminates the sample with coherent monochromatic laser light and a phase image is recorded by a CCD camera. Further details on the setup can be found in Ref. 34. As the sample holder in the microscope setup, a heating stage was used, which opens the possibility to monitor molecular annealing-kinetics in real space. For comparison, atomic force microscopy (AFM) images with calibrated height resolution were recorded with an *Autoprobe CP* from *Park Scientific Instruments*.[35] While AFM offers superior resolution, our reflection optical microscope has higher temporal resolution, greater thermal stability, and it can also collect morphological information of very soft or even molten molecular films.

The grown and annealed films were subsequently analyzed in different x-ray geometries. Grazing incidence wide angle x-ray scattering patterns have been recorded at the P03 beamline PETRA III at DESY, Hamburg at a wavelength of 0.957 Å.[36] The 2d area detector (PILATUS 300k) images were converted to reciprocal space maps as described by Lilliu *et al.*[37] Grazing incidence x-ray diffraction (GIXD) patterns and θ-2θ scans of previously annealed samples were recorded at ESRF ID03 beamline with 1.31 Å wavelength.[38] All x-ray measurements have been performed at room temperature under nitrogen atmosphere unless stated differently. The temperature measurements of the *in situ* x-ray and the microscopy setup differed by about 2 K and we estimate the overall error in the temperature measurements to be ±5 K.

RESULTS AND DISCUSSION

Evaporated TTC thin films undergo significant morphological and structural changes during thermal annealing. In
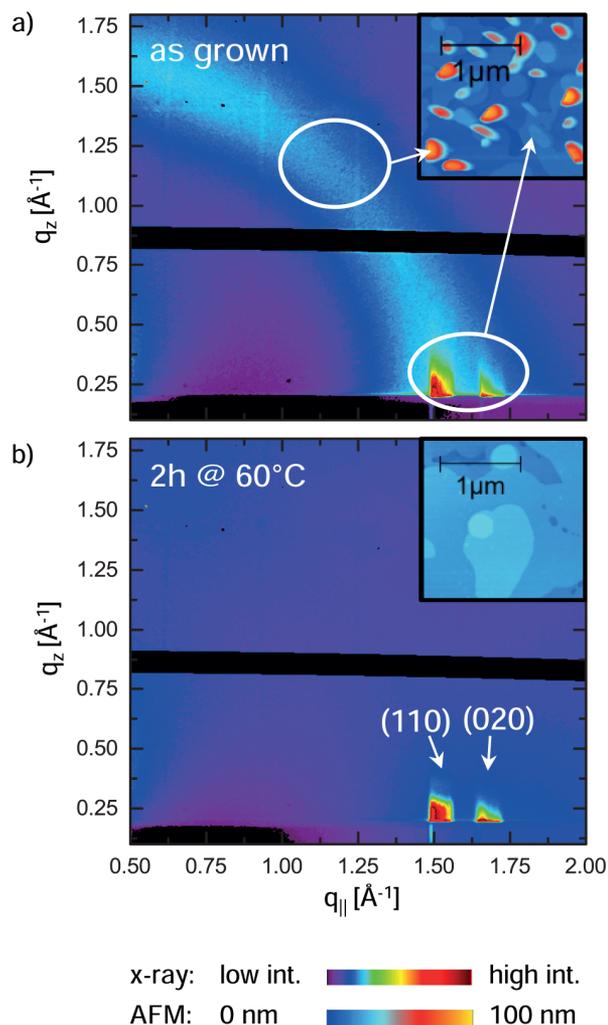

FIG. 1. (a) GIXD pattern of TTC grown at RT shows intense Bragg (110) and (020) Bragg reflections of textured, crystalline islands and a powder diffraction ring originating from randomly oriented crystalline mounds (inset: AFM image showing an area where both crystalline species appear). (b) GIXD and AFM of the annealed sample that has been kept at 60 °C for 2 h. The mound shaped crystallites as well as the diffraction ring disappear during annealing and the lateral island size increases.

freshly grown films, TTC molecules arrange in two distinct morphologies: flat, crystalline islands with monomolecular step-edges and crystalline mounds of more than 100 nm in height (see AFM insets in Figure 1). These two morphologies have also been found by Kraus *et al.*[15] Figure 1(a) shows the GIXD pattern of the TTC film as deposited. At $q_{\parallel}$ = 1.50 Å^{-1} and $q_{\parallel}$ = 1.66 Å^{-1}, the (110) and (020) in-plane reflections are visible which can be assigned to textured, upright standing molecules with respect to the substrate. Further, a ring-shaped diffraction pattern above the (110) reflection is visible. This powder diffraction ring at $|q|$ = (1.5 ± 0.1) Å^{-1} is due to randomly oriented TTC crystallites. The ring-shaped diffraction pattern disappears when rising the film's temperature to 60 °C (Figure 1(b) and real time GIXD in the supplementary material[39]). As visible from the AFM image (Figure 1(b), inset), the mound shaped crystallites are also missing after this process. Hence, through annealing of the film, the randomly oriented crystallites disappear. This leads to the conclusion that untextured molecular crystallites
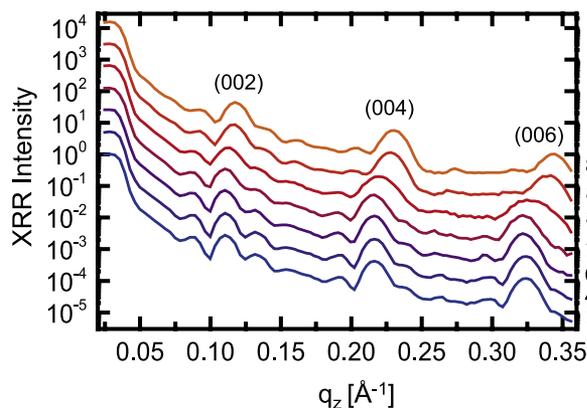
FIG. 2. *In situ* x-ray reflectivity at different substrate temperatures. A phase transition occurs between 77 °C and 83 °C, with phase coexistence at 80 °C as suggested by the increased width of the (004) and (006) Bragg reflections.
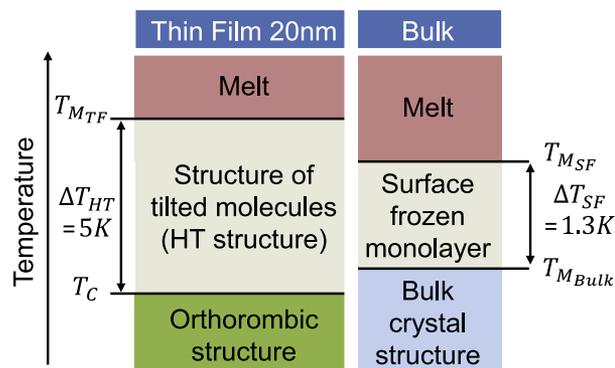

FIG. 3. Comparison between temperature dependent structures in thin films and bulk crystals that highlights the similarities between the HT structure in thin films and surface frozen monolayers. An offset in the absolute temperature values can be attributed to differing setups for thin film and bulk crystal experiments.

are located in the mound shaped structures and that they are in a thermodynamically less favorable confirmation than the underlying textured molecular film.

To study the out-of-plane structure of the textured molecular islands during the annealing process in N_2 atmosphere, we make use of *in-situ* x-ray reflectivity (XRR).[40] As shown in Figure 2, in the temperature range between 20 °C and 60 °C, we cannot find any significant changes in the reflectivity signal. Annealing in this temperature range also increases the crystallinity of the sample (see the supplementary material[39] for details). Both the films grown at room temperature as well as films heated up to 77 °C show an out-of-plane lattice spacing of (58.8 ± 0.3) Å. Together with the position of the in-plane diffraction peaks (see the supplementary material[39]), this is in agreement with the commonly known orthorhombic crystal structure (a = 4.98 Å, b = 7.44 Å, c = 115.2 Å).[7,18,23–27]

Further elevation of the substrate temperature from 77 °C to 83 °C induces a phase transition to a high temperature (HT) structure that is characterized by a significant decrease of the out-of-plane lattice spacing. At about 80 °C, both crystal polymorphs coexist, as can be seen from the increased width of the Bragg reflections in Figure 2. The new phase persists even after cooling down the sample to room temperature (see the supplementary material[39] for details), i.e., the phase transition is irreversible. For this emerging phase, we find a reduced out-of-plane lattice constant of (53.4 ± 0.3) Å similar to the lattice parameter reported by Gorce *et al.*[21] and Sullivan and Weeks[23] in single crystals. Through the reduction of the out-of-plane lattice spacing from 58.8 Å to 53.4 Å, we estimate the molecular tilt angle with respect to the surface normal to be $\varphi = 90° - \sin^{-1}(53.4/58.8) \approx 24°$. An additional in-plane diffraction peak at $q_{\parallel} = 1.47$ Å^{-1} (see the supplementary material[39]) corresponds to this HT phase. Bai *et al.* find a similar in-plane diffraction pattern for a sub-monolayer of $C_{32}H_{66}$ on Si which also emerges with increasing temperature and correlate it with surface frozen structures.[41] The new lattice spacing as well as the molecular tilt angle and the increased in-plane lattice spacing of 4.26 Å is consistent with the values found by Ocko *et al.* for the surface frozen monolayers of $C_{44}H_{90}$.[32] Therefore, we conclude that the HT structure, which emerges at a critical temperature T_C, about $\Delta T_{HT} = 5$ K below

the thin film melting point, shows apparent similarities to surface frozen monolayers existing in a temperature range $\Delta T_{SF} = 1.3$ K[32] between bulk and melting temperature of the surface frozen layer (see Figure 3). A comparable behavior can be found for $C_{30}H_{62}$ and has been correlated to its rotator phase.[42] The general similarity of molecular thin films and surface frozen monolayers found on alkane melts close to their melting temperature due to their similar dimensionality has been previously highlighted by Witte and Wöll.[43]

We performed heating cycles on TTC thin films grown at room temperature on substrates with a 300 nm SiO$_x$ layer with the aim to characterize the molecular island size evolution, which is relevant for technological use of TTC, but also serves as a model for annealing of other rod-like molecules. To gain real-time insights, the sample is monitored by reflection optical microscopy while increasing the substrate temperature (Figures 4(a)–4(d)). For reference, additional samples have been heated to 60 °C and 82 °C, respectively, and cooled down again to be analyzed by AFM (insets in Figure 4 have the same scale as the optical microscopy images). The AFM image of the as-grown sample (inset of Figure 4(a)) reveals mound shaped structures on top of the film with a smaller lateral dimension (below 300 nm) compared to the underlying molecular terraces, but with heights of 100 nm and more. These mounds are too small to be resolved in the optical microscope with a lateral resolution of 500 nm and are only visible in AFM. Heating the TTC film to 60 °C (Figure 4(b)) leads to an increased lateral grain size from about 1 μm to 5 μm and to a disappearance of the mound shaped crystallites as mentioned above. Starting at temperatures above 60 °C, the molecular islands grow significantly and reach diameters of up to 10 μm (average grain area in the order of 2.5 μm^2) at 82 °C (Figure 4(c)), which can be fully resolved with an optical microscope. In this temperature range, the phase transition to HT phase has already begun and there is phase coexistence in the film (see the supplementary material[39]). Further heating of the sample leads to the formation of liquid TTC droplets that result in Newton-rings in the microscope (Figure 4(d)) at 87 °C.

Since the optical microscopy allows us to record real time data (see Figure 4(e) and the supplementary material[39] for
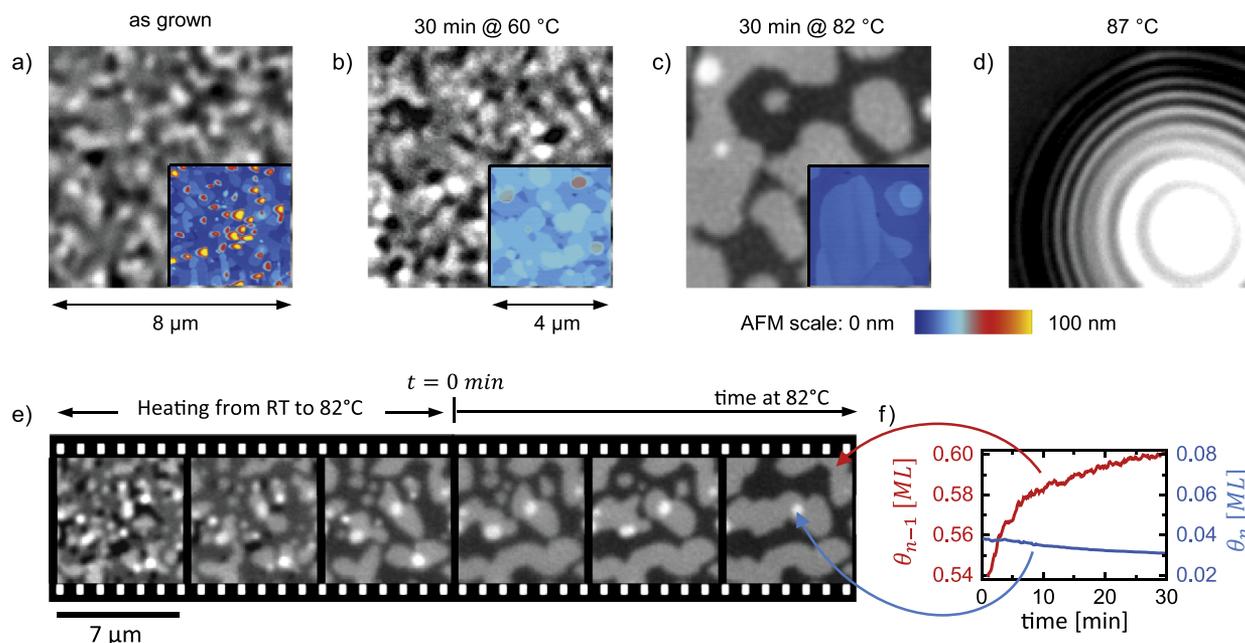
FIG. 4. Top: Reflection optical microscopy images at different temperatures and corresponding AFM images (insets) for samples that have been heated to the same temperatures and cooled down to room temperature again. Contrast from step edges of single molecular height is visible in optical microscopy. This enables a real-time observation of annealing at different temperatures, starting with coexistence of islands and mounds on top in (a), the disappearance of mounds and an increase of island size at 60 °C in (b), and a significant increase of island size at 82 °C in (c). At 87 °C, the TTC dewets into molten droplets (d). Bottom: (e) Time series of optical microscopy images highlighting the smoothing of the film. Downhill transport of molecules in layer n (monolayer (ML) coverage θ_n) fills holes in layer $n-2$ and increases layer coverage θ_{n-1} in layer $n-1$ (see graph of layer coverages (f)). Ostwald ripening leads to significantly increased island sizes in the partially filled layer $n-1$.

a movie), the individual monolayer (ML) coverage has been extracted[44] from an approximately 5000 μm^2 sized area in Figure 4(f). While the topmost layer n and higher structures depopulate over time at a rate of $-5 \cdot 10^{-4}$ ML/min at 82 °C, the underlying layer $n-1$ is filled at a rate of up to 10^{-3} ML/min. Simultaneously, the number of islands and the corresponding boundary length of both layers decrease which indicates an Ostwald ripening process. The video footage (see the supplementary material[39]) of this process clearly indicates that smaller islands coalesce with larger ones and that molecules from the topmost layer are adsorbed in underlying layers (downhill transport) resulting in a significant smoothing of the film surface. Within a few minutes at temperatures of 5 K below the melting temperature, the lateral dimension of ML height islands increases drastically up to 10 μm in diameter. Bai *et al.* have observed a similar behavior in the case of $C_{30}H_{62}$ close to its melting point.[41] Focusing on the lateral structure, the model of 2d-Ostwald ripening explains the observed behavior in terms of the Gibbs-Thomson effect: smaller crystalline structures have a reduced melting temperature compared to larger ones due to their higher fraction of surface atoms.[45] According to this theory, a molecular island suddenly dissolves completely once its size falls below a certain limit[46] — a behavior clearly observable in our real-time microscopy data (see the supplementary material[39]).

Compared with other molecules such as pentacene (PEN),[47,48] PTCDA,[49] or oligothiophenes,[2] which tend to roughen when heated to elevated temperatures, the 2d-ripening and smoothing of a crystalline n-alkane thin film during annealing is unexpected. In what follows, we contrast the molecular kinetics and energetics of TTC with PEN, as a prototypical molecule in organic thin film growth[50] that does not show thermal smoothing but surface roughening.

During the annealing process, the kinetics play an important role, so that it is instructive to compare growth speeds in different crystallographic directions because fast lateral and slow vertical growth favors 2d ripening. Already the equilibrium crystal shape points to the fact that TTC grows more in 2d fashion as its equilibrium shape is plate-like[51,52] in contrast to the more 3d equilibrium crystal shape of PEN.[53] Further, during the annealing process, the growth speeds are governed by the attachment energies and intermolecular forces of molecules to different crystal facets, which we calculated in a simple Coulomb-London-Pauli force-field model.[54] For TTC, we find the head-to-tail attachment energy to be only -2.5 kJ/mol while lateral attachment is strongly favored at -334.0 kJ/mol. For pentacene in its bulk structure, we calculated the respective attachment energies to be -12.9 kJ/mol *vs.* -256.9 kJ/mol. The much stronger anisotropy in attachment energies of TTC (1:140) in contrast to PEN (1:20) contributes to the observed smoothing of TTC films.

Beyond kinetics, the energetics of TTC and PEN as well as the substrate surface have to be considered, since a lowering of the surface and interface energies are major contributions to the minimization of the Gibbs free energy during annealing. Under annealing conditions, PEN exhibits a phase transition from an orthorhombic thin film (TF) phase towards its triclinic bulk crystal structure. This phase transition goes hand in hand with a morphological change that lowers the pentacene surface/volume ratio by forming 3d crystals instead of a continuous film. As a result, the total surface
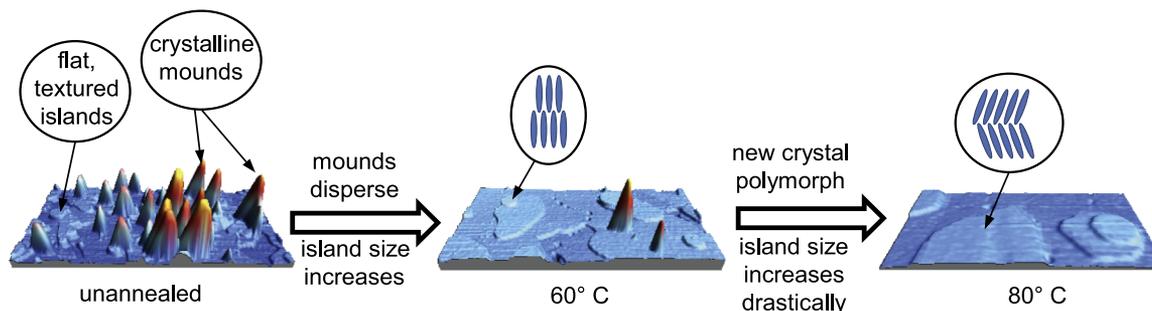
FIG. 5. Sketch of the TTC surface morphology at different temperatures with indicated crystal structures.

energy increases whereas this loss is more compensated by the reduction of the volume Gibbs free energy in the bulk phase.[55] The observed smoothening of the TTC film in contrast leads to the conclusion that in this case the reduction of the surface energy plays the dominating role and that the volume Gibbs free energy does not change much during the observed phase transition towards the HT phase.

Taking a closer look at the surface energies of PEN and TTC, a notable difference can be found in the absolute values of the surface energies that range between 50 mJ/m^2 and 150 mJ/m^2 depending on the crystal facet for PEN[56] and between 20 mJ/m^2 and 30 mJ/m^2 in the case of TTC.[57] This difference in the surface energies explains the distinct wetting behavior of alkanes and aromatic molecules like PEN on silica surfaces, which has a surface energy of (57.5 ± 14) mJ/m^2.[58] With its low surface energy, TTC is driven to wet both the SiO$_2$ substrate and underlying alkane layers, as demonstrated by Lazar *et al.* for C$_{30}$H$_{60}$ und C$_{36}$H$_{74}$.[31] In this study, also the coexistence of a crystalline alkane phase and a liquid phase has been observed, in contrast to PEN where only solid phases have been found for the given annealing conditions.[59] This qualitative difference is important in the context of ripening and surface smoothing as the liquid phase allows for significant mass transport across several μm.

CONCLUSION

Our results quantify the variety of technologically relevant morphological and structural changes that TTC thin films undergo during annealing. As illustrated in Figure 5, we identify two stages in the annealing process of TTC films grown at 20 °C that consist of both flat 2d islands and 3d mounds. First, the crystalline mounds disappear at around 60 °C and, second, above 80 °C, the lateral dimension of the TTC islands increases significantly and an irreversible phase transition occurs. We find a remarkable smoothing and strong lateral growth of flat islands which results from annealing TTC thin films at temperatures close to the melting point. The use of a phase contrast optical microscope enables us for the first time to follow the annealing and downward flux across step edges of alkane molecules in evaporated multilayer films and demonstrates the promise of this technique for real time growth studies. The flat molecular structures on large lateral scales are particularly promising for the technological use of TTC as a planar insulating layer and a template for pseudoepitaxial growth of other organic semiconductors on top. We identify

the anisotropic binding energies and low surface energies as key parameters for the favorable annealing properties. This improves the understanding of organic thin film growth and might help to tailor molecules with desired wetting properties.

[1]O. A. Melville, B. H. Lessard, and T. P. Bender, ACS Appl. Mater. Interfaces **7**, 13105 (2015).
[2]A. Zen, P. Pingel, D. Neher, and U. Scherf, Phys. Status Solidi A **205**, 440 (2008).
[3]P. Beyer, T. Breuer, S. Ndiaye, A. Zykov, A. Viertel, M. Gensler, J. P. Rabe, S. Hecht, G. Witte, and S. Kowarik, ACS Appl. Mater. Interfaces **6**, 21484 (2014).
[4]A. Hinderhofer, T. Hosokai, K. Yonezawa, A. Gerlach, K. Kato, K. Broch, C. Frank, J. Novák, S. Kera, N. Ueno, and F. Schreiber, Appl. Phys. Lett. **101**, 033307 (2012).
[5]C. Merkl, T. Pfohl, and H. Riegler, Phys. Rev. Lett. **79**, 4625 (1997).
[6]A. Holzwarth, S. Leporatti, and H. Riegler, Europhys. Lett. **52**, 653 (2000).
[7]S. R. Craig, G. P. Hastie, K. J. Roberts, and J. N. Sherwood, J. Mater. Chem. **4**, 977 (1994).
[8]C. Weber, T. Liebig, M. Gensler, L. Pithan, S. Bommel, D. Bléger, J. P. Rabe, S. Hecht, and S. Kowarik, Macromolecules **48**, 1531 (2015).
[9]J. L. Lee, E. M. Pearce, and T. K. Kwei, Macromolecules **30**, 8233 (1997).
[10]M. Göllner, M. Huth, and B. Nickel, Adv. Mater. **22**, 4350 (2010).
[11]D.-I. Kim, T. Q. Trung, B.-U. Hwang, J.-S. Kim, S. Jeon, J. Bae, J.-J. Park, and N.-E. Lee, Sci. Rep. **5**, 12705 (2015).
[12]M. Kraus, S. Richler, A. Opitz, W. Brütting, S. Haas, T. Hasegawa, A. Hinderhofer, and F. Schreiber, J. Appl. Phys. **107**, 094503 (2010).
[13]S. Ogawa, Y. Kimura, M. Niwano, and H. Ishii, Appl. Phys. Lett. **90**, 033504 (2007).
[14]M. Irimia-Vladu, E. D. Głowacki, P. A. Troshin, G. Schwabegger, L. Leonat, D. K. Susarova, O. Krystal, M. Ullah, Y. Kanbur, M. A. Bodea, V. F. Razumov, H. Sitter, S. Bauer, and N. S. Sariciftci, Adv. Mater. **24**, 375 (2012).
[15]M. Kraus, S. Haug, W. Brütting, and A. Opitz, Org. Electron. **12**, 731 (2011).
[16]M. Horlet, M. Kraus, W. Brütting, and A. Opitz, Appl. Phys. Lett. **98**, 233304 (2011).
[17]A. Opitz and W. Brütting, in *Physics of Organic Semiconductors*, edited by W. Brütting and C. Adachi (Wiley-VCH, Weinheim, Germany, 2013), pp. 239–265.
[18]C. Weber, C. Frank, S. Bommel, T. Rukat, W. Leitenberger, P. Schäer, F. Schreiber, and S. Kowarik, J. Chem. Phys. **136**, 204709 (2012).

[19] A. Müller, Proc. R. Soc. A **127**, 417 (1930).

[20] A. Müller, Proc. R. Soc. A **138**, 514 (1932).

[21] J. Gorce, S. J. Spells, X. Zeng, and G. Ungar, J. Phys. Chem. B **108**, 3130 (2004).

[22] M. Dirand, M. Bouroukba, A.-J. Briard, V. Chevallier, D. Petitjean, and J.-P. Corriou, J. Chem. Thermodyn. **34**, 1255 (2002).

[23] P. K. Sullivan and J. J. Weeks, J. Res. Natl. Bur. Stand., Sect. A **74A**, 203 (1970).

[24] P. K. Sullivan, J. Res. Natl. Bur. Stand., Sect. A **78A**, 129 (1974).

[25] O. Phaovibul, H. Čačković, J. Loboda-Čačković, and R. Hosemann, J. Polym. Sci., Part A-2: Polym. Phys. **11**, 2377 (1973).

[26] B. G. Rånby, F. F. Morehead, and N. M. Walter, J. Polym. Sci. **44**, 349 (1960).

[27] A. Briard, M. Bouroukba, D. Petitjean, N. Hubert, and M. Dirand, J. Chem. Eng. Data **48**, 497 (2003).

[28] M. Dirand, M. Bouroukba, V. Chevallier, D. Petitjean, E. Behar, and V. Ruffier-Meray, J. Chem. Eng. Data **47**, 115 (2002).

[29] A. Tkachenko and Y. Rabin, Phys. Rev. Lett. **76**, 2527 (1996).

[30] H. Schollmeyer, B. Struth, and H. Riegler, Langmuir **19**, 5042 (2003).

[31] P. Lazar, H. Schollmeyer, and H. Riegler, Phys. Rev. Lett. **94**, 116101 (2005).

[32] B. M. Ocko, X. Z. Wu, E. B. Sirota, S. K. Sinha, O. Gang, and M. Deutsch, Phys. Rev. E **55**, 3164 (1997).

[33] B. M. Ocko, E. B. Sirota, M. Deutsch, E. DiMasi, S. Coburn, J. Strzalka, S. Zheng, A. Tronin, T. Gog, and C. Venkataraman, Phys. Rev. E **63**, 032602 (2001).

[34] R. Köhler, P. Lazar, and H. Riegler, Appl. Phys. Lett. **89**, 241906 (2006).

[35] D. Nečas and P. Klapetek, Cent. Eur. J. Phys. **10**, 181 (2012).

[36] A. Buffet, A. Rothkirch, R. Döhrmann, V. Körstgens, M. M. Abul Kashem, J. Perlich, G. Herzog, M. Schwartzkopf, R. Gehrke, P. Müller-Buschbaum, and S. V. Roth, J. Synchrotron Radiat. **19**, 647 (2012).

[37] S. Lilliu, T. Agostinelli, E. Pires, M. Hampton, J. Nelson, and J. E. Macdonald, Macromolecules **44**, 2725 (2011).

[38] O. Balmes, R. van Rijn, D. Wermeille, A. Resta, L. Petit, H. Isern, T. Dufrane, and R. Felici, Catal. Today **145**, 220 (2009).

[39] See supplementary material at http://dx.doi.org/10.1063/1.4934501 for real time microscopy and GIXD video footage as well as additional x-ray diffraction results.

[40] M. Sparenberg, A. Zykov, P. Beyer, L. Pithan, C. Weber, Y. Garmshausen, F. Carlà, S. Hecht, S. Blumstengel, F. Henneberger, and S. Kowarik, Phys. Chem. Chem. Phys. **16**, 26084 (2014).

[41] M. Bai, K. Knorr, M. J. Simpson, S. Trogisch, H. Taub, S. N. Ehrlich, H. Mo, U. G. Volkmann, and F. Y. Hansen, Europhys. Lett. **79**, 26003 (2007).

[42] H. Schollmeyer, B. Ocko, and H. Riegler, Langmuir **18**, 4351 (2002).

[43] G. Witte and C. Wöll, J. Mater. Res. **19**, 1889 (2004).

[44] W. S. Rasband, U. S. National Institutes Health, Bethesda, Maryland, USA, 2015, http://imagej.nih.gov/ij/.

[45] H. Brune, in *Surface and Interface Science*, edited by K. Wandelt (Wiley-VCH, 2014), pp. 421–492.

[46] C. Wagner, Z. Elektrochem **65**, 581 (1961).

[47] T. Ji, S. Jung, and V. K. Varadan, Org. Electron. **9**, 895 (2008).

[48] R. Ye, M. Baba, K. Suzuki, Y. Ohishi, and K. Mori, Jpn. J. Appl. Phys., Part 1 **42**, 4473 (2003).

[49] B. Krause, A. C. Dürr, F. Schreiber, H. Dosch, and O. H. Seeck, J. Chem. Phys. **119**, 3429 (2003).

[50] S. Kowarik, A. Gerlach, W. Leitenberger, J. Hu, G. Witte, C. Wöll, U. Pietsch, and F. Schreiber, Thin Solid Films **515**, 5606 (2007).

[51] P. Bennema, X. Y. Liu, K. Lewtas, R. D. Tack, J. J. M. Rijpkema, and K. J. Roberts, J. Cryst. Growth **121**, 679 (1992).

[52] P. J. C. M. van Hoof, R. F. P. Grimbergen, H. Meekes, W. J. P. van Enckevort, and P. Bennema, J. Cryst. Growth **191**, 861 (1998).

[53] T. Kakudate, N. Yoshimoto, and Y. Saito, Appl. Phys. Lett. **90**, 081903 (2007).

[54] A. Gavezzotti, New J. Chem. **35**, 1360 (2011).

[55] C. C. Yang, S. Li, and J. Armellin, J. Phys. Chem. C **111**, 17512 (2007).

[56] L. F. Drummy, P. K. Miska, D. Alberts, N. Lee, and D. C. Martin, J. Phys. Chem. B **110**, 6066 (2006).

[57] X. Z. Wu, B. M. Ocko, E. B. Sirota, S. K. Sinha, M. Deutsch, B. H. Cao, and M. W. Kim, Science **261**, 1018 (1993).

[58] P. R. Ribič, V. Kalihari, C. D. Frisbie, and G. Bratina, Phys. Rev. B **80**, 115307 (2009).

[59] J. E. Goose, K. Wong, P. Clancy, and M. O. Thompson, Appl. Phys. Lett. **93**, 10 (2008).